Momentum-resolved photoelectron interference in crystal surface barrier scattering

Aimo Winkelmann,[1,*] Martin Ellguth,[1] Christian Tusche,[1] A. Akin Ünal,[1] Jürgen Henk,[2] and Jürgen Kirschner[1]
[1]*Max-Planck-Institut für Mikrostrukturphysik, Weinberg 2, 06120 Halle, Germany*
[2]*Martin-Luther-Universität Halle-Wittenberg, Institut für Physik, FG Theoretische Physik, Von-Seckendorff-Platz 1, 06120 Halle, Germany*
(Received 4 April 2012; published 16 August 2012)

The quantum-mechanical transmission process of a photoelectron through a surface leaves distinctive marks in the electron momentum distribution emitted from a crystal. By energy-resolved measurements of the complete photoemission half-space above a Cu(001) surface using a momentum microscope, we identify the two-path interference of directly emitted photoelectrons and electrons, which have been scattered through the surface quantum well via a diffraction process. The basic principle of photoelectron surface barrier interference is revealed by an analytical model. A quantitative comparison to the experiment is obtained by one-step photoemission calculations for different surface barrier models.

DOI: 10.1103/PhysRevB.86.085427 PACS number(s): 61.05.J−, 79.60.−i, 73.20.−r

I. INTRODUCTION

The surface of a crystal, which forms the transition region between the interior, three-dimensionally periodic potential and the surrounding vacuum, is an important model system for the study of electronic states and their interactions in environments of reduced symmetry. As one of the simplest examples, electrons can become trapped in front of a crystal surface in an effective surface barrier quantum well and form a Rydberg-like series of unoccupied image potential (IP) states below the vacuum level.[1] These surface barrier induced image potential states are usually sensed by inverse photoemission, scanning tunneling spectroscopy (STS), and two-photon photoemission (2PPE). Electron spectroscopic techniques like 2PPE give access to energy domain quantum interference effects at the surface, which include the recently demonstrated Fano effect at Si(001) surfaces[2] and quantum-mechanical trapping of image-potential resonances at Al(001) surfaces.[3] In the time domain, quantum interference for excited states in the surface barrier has been demonstrated using 2PPE by the observation of time-resolved quantum beats.[4] Real-space interference of IP states is seen in spatially resolved STS measurements.[5]

In comparison to surface barrier interference effects in the spatial, energy, and time domains, in this report we demonstrate momentum domain interference for photoelectrons transmitted through the surface barrier. In our approach we measure photoelectrons that have been excited well *above* the vacuum threshold by photons with energies in the order of 20 eV. While it may seem that such relatively high-energy electrons are largely unaffected by the image potential energy region *below* the vacuum level, the parallel collection of energy-resolved two-dimensional (2D) photoelectron distributions using a momentum microscope[6] allows us to discriminate specific effects that couple the excited photoelectrons above the vacuum level to the region of quasibound states in the surface potential below the vacuum level. For a Cu(001) surface, we demonstrate interference between a direct photoelectron wave coming from the bulk and another part of the photoelectron wave, which is scattered in the surface potential. We discuss the implications of surface barrier scattering for a correct theoretical description of photoelectron momentum distributions.

II. EXPERIMENT

As a typical experimental observation, we show a Cu(001) photoelectron momentum map at a kinetic energy of 14.35 eV in Fig. 1, where p_x and p_y indicate the respective components of the external surface-parallel photoelectron momentum. The data in Fig. 1 and the other data presented in this report were measured using a momentum microscope, which is an advanced combination of a photoelectron emission microscope (PEEM) column with an aberration-corrected electrostatic electron energy analyzer (energy resolution <200 meV and momentum resolution ≈0.035 Å^{-1}).[6] The instrument can record in a single run the energy-resolved and (p_x,p_y)-resolved photoemission intensity in the whole emission half-space. The electrons emitted normal to the surface appear at $(p_x,p_y)=0$, and electrons emitted nearly parallel to the surface plane show up in the outer perimeter of the circular region in Fig. 1, which corresponds to a maximum possible photoelectron wave number of $|\boldsymbol{p}_\parallel|/\hbar = 1.93$ Å^{-1} for the kinetic energy of 14.35 eV.[7] For comparison, conventional angle-resolved photoelectron spectroscopy (ARPES) setups with two-dimensional detection usually measure the energy along one dimension and a selected angular range along the other dimension of the detector. Of course, the effects we report here are in principle also observable in the conventional setups as long as the two-dimensional k space is scanned (e.g., by sample rotation) with a sufficient resolution.

The photoemission experiments were carried out on clean Cu(001) surfaces at −100 °C using He I radiation from a nonmonochromatized and nonpolarized laboratory lamp ($h\nu = 21.2$ eV). To emphasize the fine-scale variations in the photoelectron momentum patterns and to remove the underlying intensity variations on a large angular scale, we divided the data by a slowly varying background obtained by a convolution of the initial pattern with a sufficiently broad Gaussian profile (for comparison to the raw data see Ref. 8, Fig. 2).

III. RESULTS AND DISCUSSION

The photoelectrons measured in Fig. 1 originate from Cu d-band states at an energy of 2.3 eV below the Fermi level.

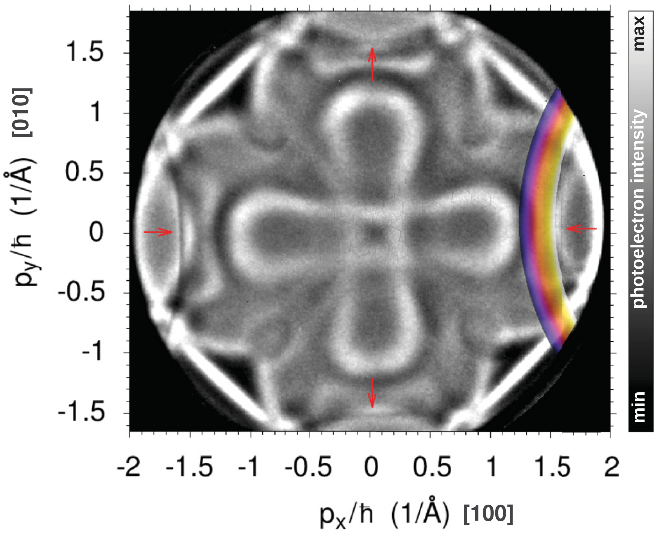

FIG. 1. (Color) Cu(001) photoelectron momentum (p_x, p_y) map at 14.35 eV kinetic energy. The arrows indicate the position of considerably sharp, arclike features. For the theoretical interpretation (see text), the colored momentum-region overlay indicates the surface-perpendicular energy $e_\perp$ [Eq. (1)] of a photoelectron near the corresponding arclike feature after diffraction by a (1,1) surface reciprocal lattice vector. The perpendicular energy ranges from -5 eV (blue side) up to the vacuum level (0 eV, white side).

These initial states determine the overall rather complicated fourfold structure of the pattern, with the [100] and [010] bulk directions defining the x and the y axis, respectively. The structure of interest for this paper is seen most clearly at the left edge of the intensity pattern in Fig. 1, where we observe an arclike dark feature which is sharper than any other structure seen in the data. As marked by the red arrows in Fig. 1, the fourfold arrangement of this special feature can also be distinguished in agreement with the symmetry of the Cu(001) surface. With an FWHM of about 0.035 Å^{-1} for the left feature, its sharpness is limited by our experimental resolution.

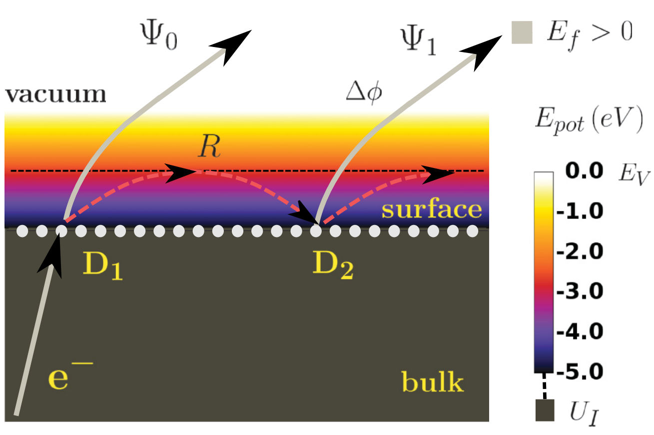

FIG. 2. (Color) Principle of photoelectron interference in the surface barrier quantum well. An excited photoelectron e^- leaving the sample is refracted due to the change between the inner potential U_I and the vacuum level (wave Ψ_0). Simultaneously, scattering at the 2D surface lattice (D_1) produces a low-angle diffracted beam (dashed red arrows), which is reflected (R) by the surface potential barrier due to a negative $e_\perp$. Diffraction process D_2 then leads back into the original direction (wave Ψ_1). The interference of Ψ_0 and Ψ_1 is governed by the phase shift $\Delta\phi$ and possible losses to the bulk states.

For the interpretation of the peculiar features, we mark a special region in Fig. 1 by a colored overlay. This defines a region in momentum space where bulk photoelectrons approaching the surface from within the crystal can be coupled into the surface barrier potential between the Fermi level and the vacuum level via a diffraction process of the surface lattice. In the region outlined by the overlay, the energy $E_\parallel$ in the parallel motion of the photoelectron after diffraction is larger than the total (kinetic) energy E_{kin} in vacuum. This results in a nominally negative energy of the diffracted beam normal to the surface,

$$e_\perp = E_{\text{kin}} - E_\parallel = E_{\text{kin}} - \frac{\hbar^2}{2m}|\boldsymbol{k}_\parallel + \boldsymbol{g}|^2, \tag{1}$$

where $e_\perp$ is measured relative to the vacuum level and $\boldsymbol{k}_\parallel = \boldsymbol{p}_\parallel/\hbar$. The emergence threshold of a diffracted beam $\boldsymbol{g}$ is defined by $e_\perp(\boldsymbol{k}_\parallel, \boldsymbol{g}) = 0$. Straightforward consideration of the scattering geometry allows to write Eq. (1) as a function of the polar emission angle θ, the azimuth ϕ, and the kinetic energy E_{kin}.[9] The overlay in Fig. 1 shows the resulting perpendicular energies from 5 eV below (blue side) and reaching up to the vacuum level (white side) for diffraction by $\boldsymbol{g} = (1,1)$. Obviously, the region near the emergence threshold of a diffracted beam seems to be correlated to the sharp features observed.

The physical picture behind Eq. (1) is sketched in Fig. 2. A photoelectron e^-, with an energy E_f above the vacuum level and excited in the bulk, is moving towards the surface. Here, the electron is refracted due to the change between the inner potential U_I and the vacuum level, resulting in a wave Ψ_0. Simultaneously, scattering at the 2D surface lattice (D_1) produces a diffracted partial wave (dashed red arrows). The angle of this beam (characterized by a reciprocal lattice vector $\boldsymbol{g}$) with respect to the surface plane can be so small that this partial wave does not have sufficient perpendicular momentum to overcome the surface barrier ($e_\perp < 0$); consequently, it is reflected (R). A second diffraction process D_2 can cause a diffracted beam with the original propagation direction (Ψ_1, with $e_\perp > 0$). The interference between the direct component Ψ_0 and the diffracted component Ψ_1 is governed by their relative phase shift $\Delta\phi$ as well as by the reflection and transmission coefficients of the bulk and vacuum side of the surface barrier quantum well. This mechanism is well known from scattering of *external* electrons in very low energy electron diffraction (VLEED), where a similar interference of a direct part Ψ_0 and a diffracted part Ψ_1 of the wave function is observed as an energy-dependent fine structure in elastic[10,11] and inelastic scattering.[12] Our observation here is that we specifically measure the momentum-dependent effects of *internally* excited photoelectrons. This means that in our experiments the phase difference $\Delta\phi$ is controlled by the direction of the momentum $\boldsymbol{p}$ of the photoelectrons at a fixed kinetic energy.

If the interpretation of our measurements in terms of the mechanism shown in Fig. 2 is correct, the momentum-dependent interference features should show a specific energy dependence irrespective of the underlying primary

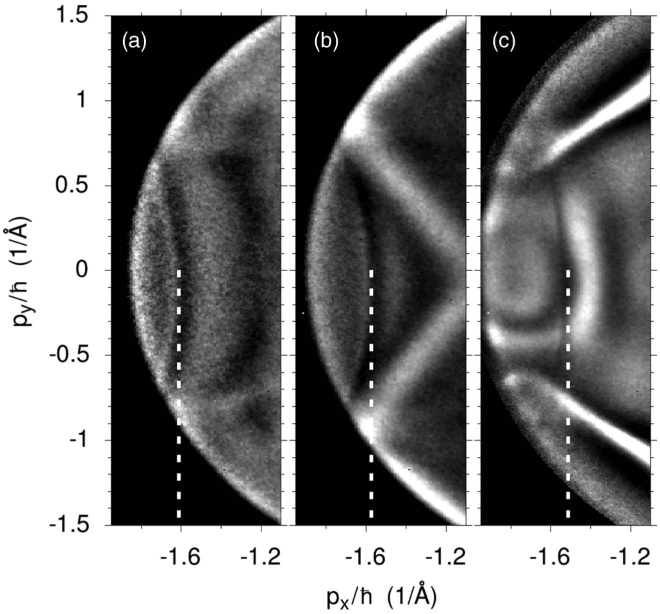

FIG. 3. Experimentally observed interference features from d-band photoelectrons of Cu(001) for final-state kinetic energies of 13.20 eV (a), 13.80 eV (b), and 14.75 eV (c) using He I excitation. The dashed lines mark the theoretically expected $\boldsymbol{p}_y = 0$ emergence threshold position of the $(\bar{1},\bar{1})$ beam for the respective energy.

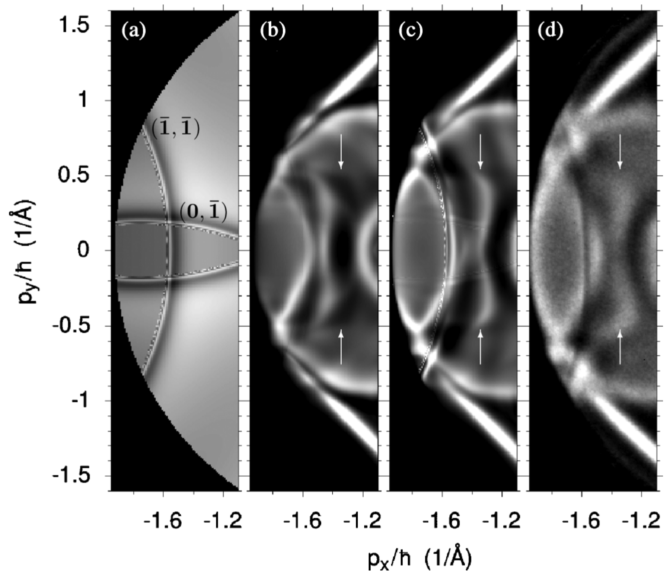

FIG. 4. Theoretical interference fine structures from Cu(001) at $E_{\mathrm{kin}} = 14.35$ eV. (a) Analytic interference model for scattering by $(\bar{1},\bar{1})$ and $(0,\bar{1})$ reciprocal lattice vectors, (b) steplike surface potential, and (c) saturated image-potential barrier (Ref. 15). (d) Experimental data reproduced from Fig. 1. Arrows indicate intensity features discussed in the text.

photoelectron intensity distribution. In order to confirm this, in Fig. 3 we show additional momentum patterns, which were measured at kinetic energies of 13.20 eV [Fig. 3(a)], 13.80 eV [Fig. 3(b)], and 14.75 eV [Fig. 3(c)]. As can be seen by the dashed lines, the $p_y = 0$ position of the arclike feature is moving toward smaller in-plane p_x momentum with increasing kinetic energy. The dashed lines in Fig. 3 are drawn at the theoretically expected $e_{\perp} = 0$ beam emergence threshold for the $(\bar{1},\bar{1})$ reflection from the simple model of Eq. (1), which results in values of -1.61 Å^{-1} [Fig. 3(a)], -1.57 Å^{-1} [Fig. 3(b)], and -1.51 Å^{-1} [Fig. 3(c)]. The experimentally observed positions of the energy-dependent structures are in very good agreement with these predictions. This confirms that the sharp features we observe are not intrinsically caused by the initial Cu d-band electronic structure.

So far, we have seen strong experimental indications that the observed properties of the arclike features are consistent with an interference mechanism based on photoelectron scattering in the surface barrier. As we will show now, the quantitative momentum-space extension and intensity of these peculiar features can be explained with theoretical models of increasing sophistication. First, modifying an analytic model for interference effects near an emergence threshold of a diffracted beam in VLEED,[9] we calculated the photoemission interference effects for a hypothetical isotropic electron emitter as a function of emission angle. We considered a perfect fcc Cu(001) surface with a bulk lattice constant of 3.61 Å, and for the generic interference parameters we took values that are consistent with the energy-dependent fine structure observed in VLEED from Cu(001).[13] For the scattering phase shifts of the bulk and the vacuum side of the barrier, we applied the analytic forms for a nearly free electron energy gap of the bulk potential and of an image-potential-like surface barrier, respectively.[14] The relevant scattering energy scale for the interference processes is the final state kinetic energy E_{kin} of the photoelectrons.

For the relevant reciprocal lattice vectors $\boldsymbol{g}$ in Eq. (1) we considered all symmetry-equivalent $(\bar{1},\bar{1})$ and $(0,\bar{1})$ vectors. As we can see in Fig. 4(a), already this simple model indeed predicts arclike fine structures from the $(\bar{1},\bar{1})$ vectors at the position we observe in the experimental data [shown in Fig. 4(d)]. Currently, the experimental energy and momentum resolution does not allow us to distinguish the increasingly fine structure that is expected in the immediate vicinity of the beam threshold. Nevertheless, the comparison to the colored overlay in the full momentum map in Fig. 1 yields that the analytic $(\bar{1},\bar{1})$ interference structure correctly converges towards the perpendicular energy vacuum level (white edge of the colored region in Fig. 1). In addition to the consistently explained $(\bar{1},\bar{1})$ arcs, the analytic interference model also predicts similar features from the $(0,\bar{1})$ reflection. These additional features are, however, not seen in our experimental data. Because the generic interference model neither incorporates information on the relative intensity of the interference features, nor describes the effects of the surface barrier relative to the underlying initial-state structure, a quantitative analysis of the experimental observations calls for first-principles theoretical photoemission calculations.

We have thus carried out photoemission calculations in the one-step model, which rely on the local density approximation (LDA) to density functional theory with a relativistic multiple-scattering approach (layer-Korringa-Kohn-Rostoker, LKKR).[16,17] To describe the initial-state d-band photoemission, we used scattering potentials obtained from an extended theoretical analysis of Cu photoemission momentum patterns in the complete valence band region.[8] The theoretical calculations allow us to consider various types of surface barrier models. Here, we focus on two selected types. In Fig. 4(b) we show the intensity for an abruptly terminated bulk potential with a potential step to the vacuum level at the last atomic layer. For this barrier model, no pronounced fine-structure effects can be distinguished. As a second, more realistic choice, we applied the model of a "saturated image barrier,"[15] which combines the long-range limit of an imagelike potential with a transition region where the image character weakens and turns to the inner potential of the bulk. For the parameters of this barrier we have taken published values obtained from VLEED experiments,[15] with the image plane at $z_{\mathrm{im}} = 2.0$ Å in front of the first row of atoms. In clear contrast to the step potential, the saturated image barrier [Fig. 4(c)] nicely confirms the interference features expected from the analytical model. Moreover, the result also shows that the additional $(0,\bar{1})$ features should be much weaker than the strong features from the $(\bar{1},\bar{1})$ vector, which consistently explains the absence of the $(0,\bar{1})$ features in our experimental data.

Apart from the fine-scale interference features near the actual beam emergence threshold, the one-step calculations for the two different barrier models also emphasize the general necessity of including a correct surface barrier. This can be seen by the overall better agreement of the calculated pattern for the imagelike barrier in the region indicated by the white arrows in Fig. 4(c). In this area, the step potential in Fig. 4(b) shows a significantly different intensity distribution, which does not fit to the experimental observations. Very interestingly, the region marked by the arrows in Fig. 4(c) closely coincides with the area indicated by the colored overlay in Fig. 1. This shows that, via a coupling provided by diffraction processes, the full range of unoccupied levels for perpendicular energies below the vacuum level can in principle influence the photoemitted intensity of electrons with total energies well above the vacuum level.

Although, for the purpose of the present paper, we have not attempted a best-match theoretical fit that would need to encompass the multitude of surface barrier models discussed in the literature, it is obvious that photoemission momentum mapping provides an alternative perspective on this important problem.[13,15,18–22] We are sure that momentum-dependent photoemission provides several distinct advantages for systematic experimental investigations of surface barrier properties as compared to, for example, scattering of external electrons.[11,23,24] First of all, photoexcitation creates internal, divergent electron sources, which can be used to coherently probe a large momentum space region of electrons subjected to the surface barrier potential. As we have seen above, in our case this allows us, for example, to judge the relative momentum-dependent influence of different surface reciprocal lattice vectors at a fixed energy. Considering the intrinsically dynamical nature of the effective potential that is experienced by an electron in front of a surface, the excitation of photoelectrons also provides the option for time-resolved investigation of the surface barrier down to the attosecond time scale.[25] With the recent demonstration of parallel spin analysis in the momentum microscope,[26] the implications of the spin-dependent properties of the surface barrier on the momentum-resolved photocurrent can be investigated.

IV. SUMMARY

We have presented a direct momentum-space investigation of photoelectron interference effects, which are caused by diffraction of photoelectrons into pre-emergent beams propagating in the surface barrier potential. As we have seen, the specific quantum-mechanical effects of the surface barrier region of a crystal must be taken into account for a correct description of the angle-resolved photoemitted intensity from a crystal.

---

*winkelm@mpi-halle.mpg.de

[1] P. M. Echenique and J. B. Pendry, J. Phys. C **11**, 2065 (1978).

[2] C. Eickhoff, M. Teichmann, and M. Weinelt, Phys. Rev. Lett. **107**, 176804 (2011).

[3] M. Winter, E. V. Chulkov, and U. Höfer, Phys. Rev. Lett. **107**, 236801 (2011).

[4] U. Höfer, I. L. Shumay, Ch. Reuß, U. Thomann, W. Wallauer, and Th. Fauster, Science **277**, 1480 (1997).

[5] P. Wahl, M. A. Schneider, L. Diekhöner, R. Vogelgesang, and K. Kern, Phys. Rev. Lett. **91**, 106802 (2003).

[6] B. Krömker, M. Escher, D. Funnemann, D. Hartung, H. Engelhard, and J. Kirschner, Rev. Sci. Instrum. **79**, 053702 (2008).

[7] We label the momentum axes of our plots by $p/\hbar$ (units of Å^{-1}) in order to emphasize that we detect free electrons with a well-defined momentum $\boldsymbol{p}$ (eigenvalues of the momentum operator $\hat{p} = -i\hbar\nabla$), as compared to the crystal momentum (Bloch wave quantum number) of the relevant initial electronic states usually labeled as $\boldsymbol{k}$.

[8] A. Winkelmann, C. Tusche, A. A. Ünal, M. Ellguth, J. Henk, and J. Kirschner, New J. Phys. **14**, 043009 (2012).

[9] C. Gaubert, R. Baudoing, Y. Gauthier, and J. Rundgren, Surf. Sci. **147**, 162 (1984).

[10] E. McRae, Rev. Mod. Phys. **51**, 541 (1979).

[11] R. O. Jones and P. J. Jennings, Surf. Sci. Rep. **9**, 165 (1988).

[12] D. Rebenstorff, H. Ibach, and J. Kirschner, Solid State Commun. **56**, 885 (1985).

[13] R. E. Dietz, E. G. McRae, and R. L. Campbell, Phys. Rev. Lett. **45**, 1280 (1980).

[14] N. V. Smith, Phys. Rev. B **32**, 3549 (1985).

[15] M. N. Read, Phys. Rev. B **32**, 2677 (1985).

[16] J. Henk, in *Handbook of Thin Film Materials, Vol. 2: Characterization and Spectroscopy of Thin Films*, edited by Hari Singh Nalwa, Ch. 10 (Academic Press, San Diego, 2002), pp. 479–526.

[17] J. Braun and M. Donath, J. Phys.: Condens. Matter. **16**, S2539 (2004).

[18] R. O. Jones, P. J. Jennings, and O. Jepsen, Phys. Rev. B **29**, 6474 (1984).

[19] E. Tamura and R. Feder, Solid State Commun. **58**, 729 (1986).
[20] G. J. Hitchen, S. M. Thurgate, and P. J. Jennings, Phys. Rev. B **44**, 3939 (1991).
[21] J. Henk, W. Schattke, H. Carstensen, R. Manzke, and M. Skibowski, Phys. Rev. B **47**, 2251 (1993).
[22] E. V. Chulkov, V. M. Silkin, and P. M. Echenique, Surf. Sci. **437**, 330 (1999).
[23] J. C. H. Spence, H. C. Poon, and D. K. Saldin, Microsc. Microanal. **10**, 128 (2004).
[24] U. Weierstall, G. G. Hembree, and J. C. H. Spence, J. Phys.: Condens. Matter. **13**, 10665 (2001).
[25] A. L. Cavalieri, N. Müller, T. Uphues, V. S. Yakovlev, A. Baltuska, B. Horvath, B. Schmidt, L. Blümel, R. Holzwarth, S. Hendel, M. Drescher, U. Kleineberg, P. M. Echenique, R. Kienberger, F. Krausz, and U. Heinzmann, Nature (London) **449**, 1029 (2007).
[26] C. Tusche, M. Ellguth, A. A. Ünal, C.-T. Chiang, A. Winkelmann, A. Krasyuk, M. Hahn, G. Schönhense, and J. Kirschner, Appl. Phys. Lett. **99**, 032505 (2011).